

# Anisotropic Mean-Field Theory for Semiflexible Polymer Dynamics under Tension

Michael Hinczewski and Roland R. Netz

Department of Physics, Technical University of Munich, 85748 Garching, Germany

We introduce an anisotropic mean-field approach for the dynamics of semiflexible polymers under tension. The theory is designed to exactly reproduce the lowest order equilibrium averages of a stretched polymer, and includes the non-trivial influence of long-range hydrodynamic coupling. Validated by Brownian hydrodynamics simulations, the theory is highly accurate over a broad parameter range, even far from the weakly bending limit. It captures the change in viscoelastic response due to polymer stiffening under tension that has been observed experimentally in cytoskeletal networks.

Understanding semiflexible biopolymers under tension is relevant both *in vivo*—determining the mechanical response of cytoskeletal networks [1, 2, 3]—and *in vitro*, due to a proliferation of single-molecule techniques like optical tweezers that involve manipulating stretched DNA [4]. Yet for one of the most basic questions there is still no comprehensive, quantitatively accurate theory: what is the dynamical response of a semiflexible chain prestretched by an external force? Existing approaches are typically based on the weakly bending approximation (WBA) [5], which assumes the polymer contour remains nearly straight—strictly valid only in the limit where the persistence length  $l_p$  is much greater than the total length  $L$ , or for a large force  $F \gg k_B T/l_p$ . This has proven a highly useful simplification, widely applied in both equilibrium [5, 6, 7] and non-equilibrium [8, 9, 10] contexts for stretched semiflexible polymers. Yet such theories are of limited value in describing the complex crossovers between dynamical regimes occurring for weaker forces or more flexible chains. Moreover, most of these theories ignore long-range hydrodynamic interactions, or include them only at the level of assuming distinct longitudinal and transverse friction coefficients,  $\zeta_{\parallel} \approx \zeta_{\perp}/2$ , appropriate for a rigid rod [9]. This only renormalizes times scales, without affecting the dynamic scaling. As we will argue below, long-range interactions do have a significant influence on the dynamics even in the weakly bending limit, and must be incorporated to obtain a quantitative comparison with experiments.

In this work, we address the gaps in the existing approaches by constructing an anisotropic mean-field theory (MFT) for a semiflexible chain under tension, including hydrodynamics through a pre-averaging approximation. The solvent-mediated coupling between all points on the polymer is not an incidental element in the method, but a key to its success: the long-range interactions make the mean-field approach more realistic. In fact, at  $F = 0$ , isotropic MFT [11] is able to capture precisely the dynamics of an end-monomer in DNA strands observed through fluorescence correlation spectroscopy [12]. Without any fitting parameters, it gives an accurate description for strands  $10^2 - 10^4$  bp in length, covering a wide range between stiff and flexible chains [13]. Unlike earlier (isotropic) attempts to extend MFT to  $F \neq 0$  [14, 15, 16], our anisotropic theory is designed to yield the exact lowest-order equilib-

rium properties for directions parallel and perpendicular to the applied force, which are derived from the numerical quantum solution of the worm-like chain (WLC) model. Having fixed the correct static quantities, we show that the theory gives highly accurate and non-trivial predictions for the dynamics, validated through comparisons with Brownian hydrodynamics (BD) simulations. In particular, it reproduces the change in viscoelastic properties due to semiflexible polymer stiffening under tension, which has been observed experimentally in cytoskeletal networks put under stress either through deformation [6], or the activity of motor proteins [1].

We begin by reviewing the isotropic MFT approach to stretched semiflexible polymers [14, 15, 16], and highlighting its limitations. The starting point is the WLC Hamiltonian,  $U_{\text{WLC}} = (l_p k_B T/2) \int ds (\partial_s \mathbf{u}(s))^2 - F \hat{\mathbf{z}} \cdot \int ds \mathbf{u}(s)$ , which describes the elastic energy of a space curve  $\mathbf{r}(s)$  with contour coordinate  $0 \leq s \leq L$  and tangent vector  $\mathbf{u}(s) \equiv \partial_s \mathbf{r}(s)$  constrained by local inextensibility to  $|\mathbf{u}(s)| = 1 \forall s$ . The first term is the bending energy, parametrized by the persistence length  $l_p$ , while the second term is the external field due to a force  $F$  along the  $z$  axis. The  $|\mathbf{u}(s)| = 1$  constraint makes the dynamics of the system analytically intractable, but the partition function  $Z$ , expressed as a path integral over  $\mathbf{u}(s)$ , can be approximated through the stationary phase approach, yielding a Gaussian mean-field model. The end result is  $Z \approx \exp(-\beta \mathcal{F}_{\text{MF}}) = \int \mathcal{D}\mathbf{u} \exp(-\beta U_{\text{MF}})$ , where local inextensibility has been relaxed and the MFT Hamiltonian is:  $U_{\text{MF}} = (\epsilon/2) \int ds (\partial_s \mathbf{u}(s))^2 + \nu \int ds \mathbf{u}^2(s) + \nu_0 (\mathbf{u}^2(0) + \mathbf{u}^2(L)) - F \hat{\mathbf{z}} \cdot \int ds \mathbf{u}(s)$ . From the stationary phase condition,  $\partial_{\nu} \mathcal{F}_{\text{MF}} = \partial_{\nu_0} \mathcal{F}_{\text{MF}} = 0$ , one finds that the parameters  $\nu$  and  $\nu_0$  are functions of  $F$  and  $\epsilon$ , and act as Lagrange multipliers enforcing the global and end-point constraints  $\int ds \langle \mathbf{u}^2(s) \rangle = L$ ,  $\langle \mathbf{u}^2(0) \rangle = \langle \mathbf{u}^2(L) \rangle = 1$ . For  $F = 0$ ,  $U_{\text{MF}}$  has been studied extensively [17, 18], and setting  $\epsilon = (3/2)l_p k_B T$  it reproduces exactly the WLC tangent-tangent correlation  $\langle \mathbf{u}(s) \cdot \mathbf{u}(s') \rangle$  and related quantities. For  $F \neq 0$ , it successfully yields the known asymptotic forms for the average end-to-end extension parallel to the force:  $\langle R_z \rangle/L = 2l_p F/3k_B T$  for  $F \rightarrow 0$ , and  $\langle R_z \rangle/L = 1 - \sqrt{3k_B T/8l_p F}$  for  $F \rightarrow \infty$  [14], where  $\mathbf{R} = \int_0^L ds \mathbf{u}(s)$ . These agree with the Marko-Siggia exact result for the WLC [19], except for the factor  $3/8$ , which should be  $1/4$ .

Underlying this discrepancy is a serious problem in the

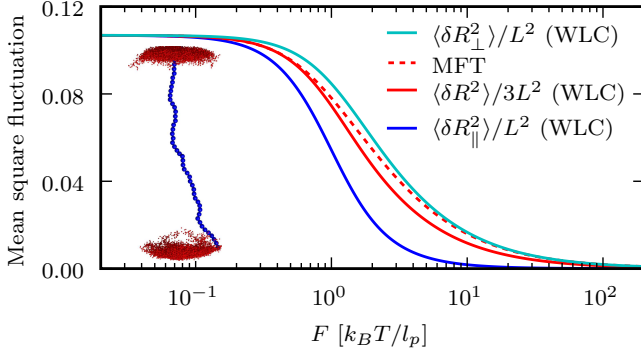


FIG. 1: (Color online) For a polymer with  $L/l_p = 5$ , the end-to-end vector fluctuation  $\langle \delta R^2 \rangle$  and its components,  $\langle \delta R_{\parallel}^2 \rangle$ ,  $\langle \delta R_{\perp}^2 \rangle$ , with varying  $F$  (derived from the exact quantum solution of the WLC), compared to the isotropic MFT prediction. Inset: cloud of end-point positions (red points) taken from a BD simulation of a polymer ( $N = 50$  beads), with  $L/l_p = 5$  and force  $F = 20 k_B T / l_p$  applied along the vertical axis. The initial polymer configuration is shown in blue.

isotropic MFT: for large  $F$  it cannot correctly account for the anisotropic fluctuation behavior of the WLC. To illustrate this, let us consider displacements  $\delta R_{\parallel} = R_z - \langle R_z \rangle$  and  $\delta R_{\perp} = R_x$  or  $R_y$ . The MFT does not differentiate between  $\parallel$  and  $\perp$  fluctuations:  $\langle \delta R_{\parallel}^2 \rangle = \langle \delta R_{\perp}^2 \rangle$  for all  $F$ . However for the WLC,  $\langle \delta R_{\parallel}^2 \rangle$  becomes much smaller than  $\langle \delta R_{\perp}^2 \rangle$ , as is evident in the inset of Fig. 1, showing a snapshot of end-point fluctuations taken from a BD simulation. A similar anisotropy exists between the  $\perp$  and  $\parallel$  fluctuations at  $F = 0$  for a stiff filament with  $L \lesssim l_p$  [20]. Using the exact mapping of the WLC onto quantum motion over the surface of a unit sphere [21], one can numerically calculate the fluctuation magnitudes, which are shown in Fig. 1. (For details see Sec. I of the supplementary material [22].) Since the MFT averages over all coordinate directions, its estimate for the magnitude converges to the exact  $\langle \delta R_{\perp}^2 \rangle$  at large  $F$ , as the  $\perp$  fluctuations dominate in that regime. It misses entirely the  $\parallel$  component. Thus to understand the dynamic response of stretched semiflexible polymers one needs a more suitable theoretical starting point.

To resolve these difficulties, we propose an anisotropic version of the Gaussian model:

$$U = \sum_{\alpha=\parallel, \perp} \left[ \frac{\epsilon_{\alpha}}{2} \int ds (\partial_s \mathbf{u}_{\alpha}(s))^2 + \nu_{\alpha} \int ds \mathbf{u}_{\alpha}^2(s) + \nu_{0\alpha} (\mathbf{u}_{\alpha}^2(0) + \mathbf{u}_{\alpha}^2(L)) \right] - \chi F \int ds u_{\parallel}(s), \quad (1)$$

with  $u_{\parallel} = u_z$ ,  $\mathbf{u}_{\perp} = (u_x, u_y)$ . We now have a total of seven parameters:  $\{\epsilon_{\alpha}, \nu_{\alpha}, \nu_{0\alpha}\}$ ,  $\alpha = \parallel, \perp$ , and a force rescaling factor  $\chi$ . The guiding philosophy will be similar to the isotropic case: to construct a Hamiltonian which closely approximates the equilibrium behavior of the WLC under tension, and then use it to derive a dynamical theory. For this purpose, we require that  $U$

should reproduce exactly the following lowest-order WLC averages:  $\langle R_{\parallel} \rangle$ ,  $\langle \delta R_{\alpha}^2 \rangle$ ,  $\int_0^L ds \langle u_{\alpha}^2(s) \rangle$ ,  $\langle u_{\alpha}^2(0) + u_{\alpha}^2(L) \rangle$ . The latter can all be calculated from the quantum solution to the WLC [22], while the corresponding analytical expressions derived from  $U$  lead to seven equations for the seven unknown parameters. These can be solved numerically for any given  $L$ ,  $l_p$ , and  $F$  (examples are shown in Sec. II of [22]). In the limit  $F \rightarrow 0$ , our approach recovers the stationary phase condition of the  $F = 0$  isotropic model, as expected.

Our dynamical theory builds on the hydrodynamic pre-averaging approach used earlier for the isotropic MFT [11, 23]. Here we give a brief outline of the approach, with the full details in Sec. III of [22]. The time evolution of the chain  $\mathbf{r}(s, t)$  is governed by the Langevin equation:  $\dot{\mathbf{r}}_{\alpha}(s, t) = - \int ds' \mu_{\text{avg}}^{\alpha}(s - s') \delta U / \delta \mathbf{r}_{\alpha}(s', t) + \xi_{\alpha}(s, t)$ , where  $\xi_{\alpha}(s, t)$  are stochastic velocities, and hydrodynamic effects are included through the pre-averaged anisotropic mobility  $\mu_{\text{avg}}^{\alpha}(s - s')$ . The latter is derived from the continuum version of the Rotne-Prager tensor  $\overleftrightarrow{\mu}(s, s'; \mathbf{x})$  [23], describing solvent-mediated interactions between two points  $s, s'$  on the contour at spatial separation  $\mathbf{x}$ . If the equilibrium probability of finding such a configuration is  $G(s, s'; \mathbf{x})$ , then the integration  $\int d^3 \mathbf{x} \overleftrightarrow{\mu}(s, s'; \mathbf{x}) G(s, s'; \mathbf{x})$  yields a diagonal  $3 \times 3$  tensor whose  $\alpha = \parallel, \perp$  components we denote as  $\mu_{\text{avg}}^{\alpha}(s - s')$ . In the absence of hydrodynamic effects (a case we will consider as a comparison), the free-draining mobility is  $\mu_{\text{fd}}^{\alpha}(s - s') = 2a\mu_0\delta(s - s')$ , where  $a$  is a microscopic length scale (i.e. the monomer radius), and  $\mu_0$  is the Stokes mobility of a sphere of radius  $a$ . We assume the stochastic velocities  $\xi(s, t)$  are Gaussian, with correlations given by the fluctuation-dissipation theorem:  $\langle \xi_{\alpha}(s, t) \xi_{\alpha}(s', t') \rangle = 2k_B T \delta(t - t') \mu_{\text{avg}}^{\alpha}(s - s')$ . The Langevin equation, together with boundary conditions at the end-points due to the applied force, can be solved through normal mode decomposition, yielding all the dynamical quantities which we will analyze below.

To validate the anisotropic MFT, we compared the theoretical results to BD simulations of a bead-spring worm-like chain, consisting of  $N$  spheres of radius  $a$  (contour length  $L = 2aN$ ), with the monomers hydrodynamically coupled through the Rotne-Prager tensor. (Full simulation details are in Sec. IV of [22]). Fig. 2 shows results for a representative semiflexible polymer, with  $L = 100a$  and  $L/l_p = 5$ . For each direction  $\alpha$ , the mean squared displacement (MSD) of the end-to-end vector,  $\Delta_{\alpha}^{\text{ee}}(t) \equiv \langle (R_{\alpha}(t) - R_{\alpha}(0))^2 \rangle$  [Fig. 2(a)], and an end-point of the chain,  $\Delta_{\alpha}^{\text{end}}(t) \equiv \langle (r_{\alpha}(L, t) - r_{\alpha}(L, 0))^2 \rangle$  [Fig. 2(b)], is depicted at two different forces  $F$ . There is excellent quantitative agreement with the BD simulations (dashed end curves), with the maximum errors  $\approx 10\%$  for the  $\perp$  and  $\approx 20\%$  for the  $\parallel$  results in the time ranges shown. The biggest discrepancies occur at short times for the  $\parallel$  component with  $F = 20 k_B T / l_p$ , where the length scale of the motion is comparable to the bead size, and we expect the discrete BD chain to deviate from continuum MFT behavior. The close agreement is all the more remarkable

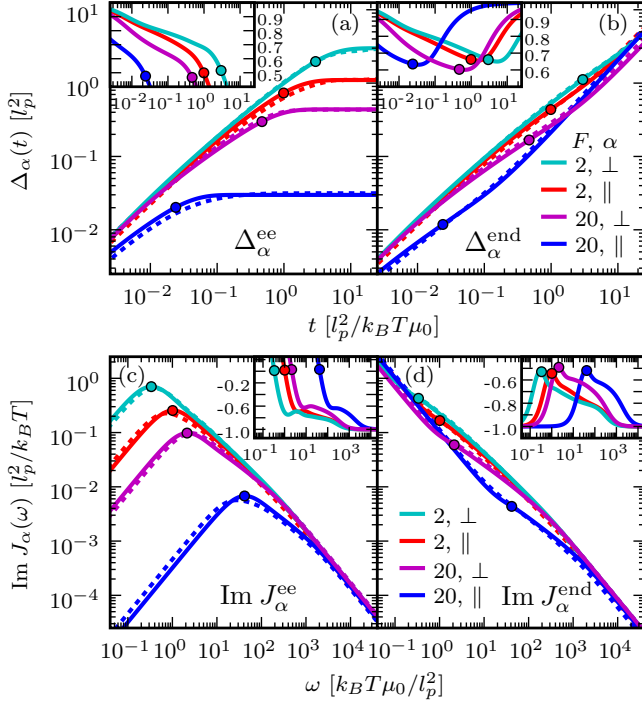


FIG. 2: (Color online) For a polymer with  $L = 100a$ ,  $L/l_p = 5$ : (a)  $\Delta_\alpha^{\text{ee}}(t)$ ; (b)  $\Delta_\alpha^{\text{end}}(t)$ ; (c)  $\text{Im} J_\alpha^{\text{ee}}(\omega)$ ; (d)  $\text{Im} J_\alpha^{\text{end}}(\omega)$ . Solid lines are the anisotropic MFT results, while dashed lines are taken from BD simulations. In all cases results are given for  $\alpha = \perp, \parallel$  at two forces,  $F = 2$  and  $20 k_B T/l_p$ . Filled circles mark the relaxation times  $\tau_{\alpha 1}$ , derived from the MFT, while the insets show the local slopes of the MFT curves in the log-log plots.

since the MSD shows a complex crossover behavior that is only imperfectly captured by asymptotic scaling theories, for example the Granek prediction [5] for  $\perp$  motion based on the WBA. For  $t \ll \tau_{\perp 1}$ , the longest relaxation time of the chain in the  $\perp$  direction, Granek derives two regimes separated by the crossover time  $t^* = 2l_p k_B T / 3F^2 \mu_0 a$ : a stiffness-dominated regime at  $t \ll t^*$ , with  $\text{MSD} \propto t^{3/4}$ , and a force-dominated regime at  $\tau_{\perp 1} \gg t \gg t^*$ , with a slower scaling  $\propto t^{1/2}$ . The insets of Fig. 2(a)-(b) show the local slopes of the log-log MSD plots,  $d \log \Delta_\alpha / d \log t$ , with times  $\tau_{\perp 1}$  calculated from the MFT marked by dots. With increasing  $F$ , we do indeed find the local slope is reduced, but the dynamic scaling is modified by two important effects: (i) the slow crossover to center-of-mass motion at times  $t \gg \tau_{\perp 1}$ , where the slopes of  $\Delta_\alpha^{\text{end}}$  and  $\Delta_\alpha^{\text{ee}}$  approach 1 and 0 respectively; (ii) logarithmic corrections due to hydrodynamics, which increase the local exponent on the order of 10%. Note that even in the strongly stretched limit,  $F l_p / k_B T \gg 1$ , where the polymer is nearly straight, hydrodynamic effects are significant. Fig. 3(a) shows MFT and BD results for  $\Delta_\alpha^{\text{end}}$  with and without hydrodynamics for a chain where  $L = 100a$ ,  $L/l_p = 5$ , and  $F = 20 k_B T/l_p$ . The MSD components in the two cases cannot be related through a simple time rescaling: for  $t^* \ll t \lesssim \tau_{\alpha 1}$ , we see clearly the expected

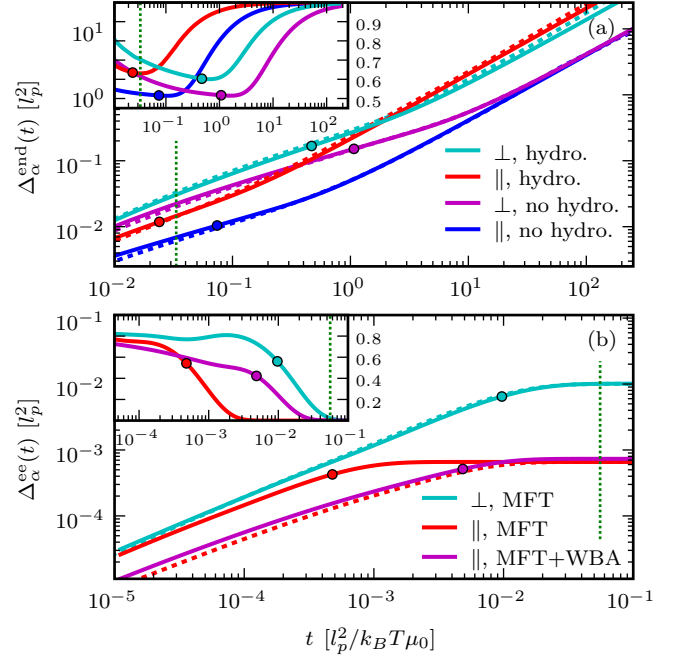


FIG. 3: (Color online) (a)  $\Delta_\alpha^{\text{end}}(t)$ ,  $\alpha = \perp, \parallel$ , for a chain with  $L = 100a$ ,  $L/l_p = 5$ ,  $F = 20 k_B T/l_p$ . The top two curves include hydrodynamic interactions, while the bottom two are free-draining. (b)  $\Delta_\alpha^{\text{ee}}(t)$  for a chain with  $L = 100a$ ,  $L/l_p = 1/3$ ,  $F = 60 k_B T/l_p$ . In both (a) and (b) MFT results are shown as solid lines, BD simulations as dashed lines. The red curve in (b) is from the combined MFT+WBA theory. The insets show the local slopes of the MFT curves in the log-log plots. MFT relaxation times  $\tau_{\alpha 1}$  are marked by circles, while the crossover times  $t^*$  are marked by vertical dashed lines.

$t^{1/2}$  behavior for the free-draining chain (local slopes are shown in the inset), while the exponent is pushed up to  $\approx 0.6 - 0.7$  with hydrodynamics.

Through the fluctuation-dissipation theorem, the MSD can be used to extract the viscoelastic properties of the chain: Fourier transforming the MSD functions gives the imaginary parts of the end-to-end and self response functions of the polymer end-points,  $\text{Im} J_\alpha^\mu(\omega) = -i\omega \Delta_\alpha^\mu(\omega) / 2k_B T$ ,  $\mu = \text{ee}, \text{end}$ , which are defined as  $J_\alpha^{\text{end}}(\omega) = \delta r_\alpha(L, \omega) / f_\alpha(\omega)$ ,  $J_\alpha^{\text{ee}}(\omega) = \delta R_\alpha(\omega) / f_\alpha(\omega)$ . Here  $\delta r_\alpha(L, \omega)$  and  $\delta R_\alpha(\omega)$  are the complex oscillation amplitudes resulting from a small force  $f_\alpha(\omega) = f_0 \exp(-i\omega t)$  applied to one or between both ends of the chain in addition to the prestretching tension  $F$ . Using the MFT, one can express  $J_\alpha^\mu(\omega)$  as a sum over normal mode contributions,  $J_\alpha^\mu(\omega) = \sum_{n=1}^{M-1} A_{\alpha n}^\mu / (1 - i\omega \tau_{\alpha n}) + \delta_{\mu, \text{end}} i D_\alpha / \omega k_B T$ , where the center-of-mass diffusion parameters  $D_\alpha$ , relaxation times  $\tau_{\alpha n}$ , and coefficients  $A_{\alpha n}^\mu$  are determined by the MFT solution [22]. The mode number cutoff  $M = L/8a$  is chosen to roughly model the discrete nature of the chain at length scales comparable to the bead diameter, but results at larger length scales are independent of the cutoff [11]. Fig. 2(c)-(d) shows  $\text{Im} J_\alpha^{\text{ee}}(\omega)$  and  $\text{Im} J_\alpha^{\text{end}}(\omega)$ , for the same param-

ters as in Fig. 2(a)-(b), compared to the results extracted from BD simulations (additional plots of the real components are in Sec. V of [22]). The good quantitative agreement with BD in the time domain is carried over to frequency space: the simulation trends are accurately reproduced by the MFT. For  $\omega \ll \tau_{\alpha 1}^{-1}$ , we see a mainly elastic end-to-end response,  $J_{\alpha}^{\text{ee}} \approx A_{\alpha 1}^{\text{ee}}(1 + i\omega\tau_{\alpha 1})$ , with an effective spring constant  $(A_{\alpha 1}^{\text{ee}})^{-1}$ . The self response of the end-point at these small frequencies is proportional to the center-of-mass mobility,  $J_{\alpha}^{\text{end}} \approx iD_{\alpha}/\omega k_B T$ . For  $\omega \gtrsim \tau_{\alpha 1}^{-1}$  we pass into the more interesting high-frequency regime governed by the complex nature of normal mode relaxation under tension and hydrodynamic interactions (up to the ultraviolet cutoff at  $\tau_{\alpha M}^{-1}$ , above which the discreteness of the chain dominates). The effects of tension in this regime have been directly observed in cytoskeletal networks through microrheology [1, 6]: with increasing force the dynamic compliance is reduced, and the high-frequency scaling changes from  $\omega^{-3/4}$  (the behavior of a relaxed semiflexible network) to  $\omega^{-1/2}$ . We find both of these stiffening effects in our MFT results, with an important correction: unlike a network, where hydrodynamics is screened, in the single polymer case the long-range interactions modify the local slopes: rather than  $-3/4$  and  $-1/2$ , we see  $\approx -0.8$  at weak force changing to  $\approx -0.6$  at strong force. This correction, along with the full crossover behavior of the imaginary response—proportional to the power spectral density (PSD)—should be observable in future nanorheology experiments for single semiflexible chains (i.e. the AFM techniques already used to extract the PSD of flexible polymers [24, 25]).

Though we have demonstrated the accuracy of the MFT, one must be careful to consider the limitations of our approach. For small forces,  $Fl_p/k_B T \ll 1$ , and extremely long chains,  $L \gg l_p^3/a^2$ , one expects self-avoidance to be important [26], which is entirely left out

of the MFT theory. (For DNA with  $l_p \approx 50$  nm, excluded volume effects would appear at  $L \gg 10^2 \mu\text{m}$ .) In the opposite limit of extremely stiff chains, with  $l_p \gg L$ , we find another problem: for a system that is nearly a rigid rod, no Gaussian model will be able to capture the  $\parallel$  dynamics. In Fig. 3(b) we show  $\Delta_{\alpha}^{\text{ee}}(t)$  for a chain with  $L = 100a$ ,  $L/l_p = 1/3$ , and  $F = 60 k_B T/l_p$ . We see that the MFT underestimates the  $\parallel$  relaxation time by an order of magnitude, saturating to equilibrium much quicker than the BD result. However the  $\perp$  Gaussian theory is still remarkably precise, deviating  $< 7\%$  from the BD curve throughout the entire time range. This provides us with an alternative solution: use the  $\perp$  MFT results in combination with WBA to estimate the  $\parallel$  quantities. The key relation is  $u_{\parallel}(s, t) \approx 1 - \mathbf{u}_{\perp}^2(s, t)$ , valid in the stiff limit. Using the  $\perp$  MFT estimate of  $\mathbf{u}_{\perp}^2(s, t)$ , we have derived a second-order perturbation expansion for  $\Delta_{\parallel}^{\text{ee}}(t)$  (details are in Sec. VI of [22]), yielding the red curve in Fig. 3(b). This gives a much better agreement with BD ( $< 25\%$  deviation). Thus with the help of WBA, we can extend the scope of our Gaussian MFT even to the rigid rod limit.

In summary, we have developed an anisotropic MFT for the dynamics of semiflexible chains under tension, whose most notable features are an unprecedented quantitative accuracy—verified through BD simulations—and a broad range of validity, not restricted to the weakly bending regime. Understanding kinetics of single stretched chains is interesting in itself (or as the first step toward more elaborate theories of stressed networks), but it can also be exploited in other contexts: optical tweezer force-clamp experiments depend sensitively on the dynamical response of the DNA handles that are attached to the object of interest, whether a nucleic acid hairpin or protein [27]. The implications of our theory in analyzing such experiments will be pursued in future work.

- 
- [1] D. Mizuno et al., *Science* **315**, 370 (2007).
  - [2] P. Bendix et al., *Biophys. J.* **94**, 3126 (2008).
  - [3] K. M. Schmoller, O. Lieleg, and A. R. Bausch, *Soft Matter* **4**, 2365 (2008).
  - [4] M. T. Woodside et al., *Science* **314**, 1001 (2006).
  - [5] R. Granek, *J. Phys. II (France)* **7**, 1761 (1997).
  - [6] A. Caspi et al., *Phys. Rev. Lett.* **80**, 1106 (1998).
  - [7] T. Hiraiwa and T. Ohta, *J. Phys. Soc. Jpn.* **77**, 023001 (2008).
  - [8] Y. Bohbot-Raviv et al., *Phys. Rev. Lett.* **92**, 098101 (2004).
  - [9] B. Obermayer et al., *Phys. Rev. E* **79**, 021804 (2009).
  - [10] O. Hallatschek, E. Frey, and K. Kroy, *Phys. Rev. Lett.* **94**, 077804 (2005).
  - [11] M. Hinczewski et al., *Macromol.* **42**, 860 (2009).
  - [12] E. P. Petrov et al., *Phys. Rev. Lett.* **97**, 258101 (2006).
  - [13] M. Hinczewski and R. R. Netz, *arXiv:0907.3891* (2009).
  - [14] B. Y. Ha and D. Thirumalai, *J. Chem. Phys.* **106**, 4243 (1997).
  - [15] L. Harnau and P. Reineker, *New J. Phys.* **1**, 3 (1999).
  - [16] R. G. Winkler, *J. Chem. Phys.* **118**, 2919 (2003).
  - [17] R. G. Winkler, P. Reineker, and L. Harnau, *J. Chem. Phys.* **101**, 8119 (1994).
  - [18] B. Y. Ha and D. Thirumalai, *J. Chem. Phys.* **103**, 9408 (1995).
  - [19] J. F. Marko and E. D. Siggia, *Macromol.* **28**, 8759 (1995).
  - [20] R. Everaers et al., *Phys. Rev. Lett.* **82**, 3717 (1999).
  - [21] J. Samuel and S. Sinha, *Phys. Rev. E* **66**, 050801 (2002).
  - [22] Supplementary material (appended after main text).
  - [23] L. Harnau, R. G. Winkler, and P. Reineker, *J. Chem. Phys.* **104**, 6355 (1996).
  - [24] Y. Sakai et al., *Appl. Phys. Lett.* **81**, 724 (2002).
  - [25] B. Khatir et al., *Biophys. J.* **92**, 1825 (2007).
  - [26] R. R. Netz and D. Andelman, *Phys. Rep.* **380**, 1 (2003).
  - [27] C. Hyeon, G. Morrison, and D. Thirumalai, *Proc. Natl. Acad. Sci. U. S. A.* **105**, 9604 (2008).

# Supplementary Material for “Anisotropic Mean-Field Theory for Semiflexible Polymer Dynamics under Tension”

Michael Hinczewski and Roland R. Netz

## I. QUANTUM SOLUTION OF THE WLC

The mapping between the WLC and a quantum particle moving on the surface of a unit sphere can be exploited to calculate exactly many of the equilibrium properties of the system [1]. Here we follow a technique similar to Ref. [2] to numerically evaluate thermodynamic averages of the WLC to arbitrary accuracy. To compute all the quantities of interest, we start with a WLC Hamiltonian augmented by two extra terms:

$$U = \frac{l_p k_B T}{2} \int_0^L ds (\partial_s \mathbf{u}(s))^2 - F \int_0^L ds u_z(s) - F_x \int_0^L ds u_x(s) - K \int_0^L ds u_z^2(s). \quad (\text{S.1})$$

The extra parameters  $F_x$  and  $K$  will later be set to zero after taking the appropriate derivatives of the partition function. Rescaling the contour variable as  $\tau = s/l_p$  and factoring out  $k_B T$ , we can rewrite  $U$  in a simpler form:

$$\beta U = \int_0^T d\tau \left[ \frac{1}{2} (\partial_\tau \mathbf{u}(\tau))^2 - f u_z(\tau) - f_x u_x(\tau) - k u_z^2(\tau) \right], \quad (\text{S.2})$$

where  $T = L/l_p$ ,  $f = \beta l_p F$ ,  $f_x = \beta l_p F_x$ , and  $k = \beta l_p K$ . Let us define the propagator  $G(\mathbf{u}_0, \mathbf{u}_T; T)$  as the path integral over all configurations with initial tangent  $\mathbf{u}(0) = \mathbf{u}_0$  and final tangent  $\mathbf{u}(T) = \mathbf{u}_T$ :

$$G(\mathbf{u}_0, \mathbf{u}_T; T) = \int_{\mathbf{u}(0)=\mathbf{u}_0}^{\mathbf{u}(T)=\mathbf{u}_T} \mathcal{D}\mathbf{u} \prod_s \delta(\mathbf{u}^2(s) - 1) \exp(-\beta U). \quad (\text{S.3})$$

Then for boundary conditions with free end-point tangents the partition function is given by  $Z = (4\pi)^{-2} \int_S d\mathbf{u}_0 d\mathbf{u}_T G(\mathbf{u}_0, \mathbf{u}_T; T)$ , where the integrations are over the unit sphere  $S$ . The quantum Hamiltonian corresponding to  $\beta U$  is

$$\mathcal{H} = -(1/2)\nabla^2 - f \cos \theta - f_x \sin \theta \cos \phi - k \cos^2 \theta, \quad (\text{S.4})$$

describing a particle on the surface of a unit sphere. In terms of the associated quantum eigenvalues  $E_n$  and eigenstates  $\psi_n(\mathbf{u})$ , the propagator  $G$  is given by:

$$G(\mathbf{u}_0, \mathbf{u}_T; T) = \sum_n e^{-E_n T} \psi_n^*(\mathbf{u}_0) \psi_n(\mathbf{u}_T) = \sum_{n,l,m,l',m'} e^{-E_n T} a_{nl'm'}^* a_{nlm} Y_{l'm'}^*(\mathbf{u}_0) Y_{lm}(\mathbf{u}_T), \quad (\text{S.5})$$

where in the second step we have expanded out the eigenstates in the basis of spherical harmonics,  $\psi_n(\mathbf{u}) = \sum_{lm} a_{nlm} Y_{lm}(\mathbf{u})$ , with coefficients  $a_{nlm}$ . For a given  $n$ , these coefficients are just the components of the  $n$ th eigenvector for the Hamiltonian  $\mathcal{H}$  in the  $Y_{lm}$  basis. Thus to proceed, one needs the detailed form of this matrix:  $\mathcal{H}_{l,m;l',m'} = \mathcal{H}_{l,m;l',m'}^0 + \mathcal{H}_{l,m;l',m'}^f + \mathcal{H}_{l,m;l',m'}^{f_x} + \mathcal{H}_{l,m;l',m'}^k$ . We list below only the nonzero elements of each contribution that are relevant to the calculation, with symmetry of the matrix implicitly assumed:

$$\begin{aligned} \mathcal{H}_{l,0;l,0}^0 &= l(l+1), & \mathcal{H}_{l,0;l+1,0}^f &= -f(l+1)[(2l+1)(2l+3)]^{-1/2}, \\ \mathcal{H}_{l,0;l,0}^k &= -\frac{k(2l(l+1)-1)}{4l(l+1)-3}, & \mathcal{H}_{l,0;l+2,0}^k &= -\frac{k(l+1)(l+2)}{(2l+3)\sqrt{4l^2+12l+5}}, \\ \mathcal{H}_{l,m;l+1,m+1}^{f_x} &= \frac{1}{2} f_x \sqrt{\frac{(l+m+1)(l+m+2)}{4l(l+2)+3}}, & \mathcal{H}_{l,m;l+1,m-1}^{f_x} &= -\frac{1}{2} f_x \sqrt{\frac{(l-m+1)(l-m+2)}{4l(l+2)+3}}. \end{aligned} \quad (\text{S.6})$$

The eigenvectors  $a_{nlm}$  and eigenvalues  $E_n$  can be readily calculated numerically by truncating the infinite matrix  $\mathcal{H}_{l,m;l',m'}$  to a finite size (with cutoff chosen large enough to get the desired precision). The partition function  $Z$  can then be written as:

$$Z = \frac{1}{(4\pi)^2} \int_S d\mathbf{u}_0 d\mathbf{u}_T \sum_{n,l,m,l',m'} e^{-E_n T} a_{nl'm'}^* a_{nlm} Y_{l'm'}^*(\mathbf{u}_0) Y_{lm}(\mathbf{u}_T) = \frac{1}{4\pi} \sum_n e^{-E_n T} a_{n00}^* a_{n00} \quad (\text{S.7})$$

Most of the thermodynamic averages used in the anisotropic MFT can be directly derived from  $Z$ :

$$\begin{aligned} \langle R_{\parallel} \rangle &= l_p \frac{\partial}{\partial f} \log Z \Big|_{f_x=0, k=0}, & \int_0^L ds \langle u_{\parallel}^2(s) \rangle &= L - \int_0^L ds \langle u_{\perp}^2(s) \rangle = l_p \frac{\partial}{\partial k} \log Z \Big|_{f_x=0, k=0}, \\ \langle \delta R_{\parallel}^2 \rangle &= l_p^2 \frac{\partial^2}{\partial f^2} \log Z \Big|_{f_x=0, k=0}, & \langle \delta R_{\perp}^2 \rangle &= 2l_p^2 \frac{\partial^2}{\partial f_x^2} \log Z \Big|_{f_x=0, k=0}. \end{aligned} \quad (\text{S.8})$$

The end-point averages are calculated similarly:

$$\langle u_{0\parallel}^2(0) + u_{0\parallel}^2(L) \rangle = 2 - \langle u_{0\perp}^2(0) + u_{0\perp}^2(L) \rangle = \frac{2}{(4\pi)^2} \int_S d\mathbf{u}_0 d\mathbf{u}_T u_{0\parallel}^2 G(\mathbf{u}_0, \mathbf{u}_T; T) = \sum_n e^{-E_n T} a_{n00}^* \left( \frac{a_{n00}}{6\pi} + \frac{a_{n20}}{3\sqrt{5}\pi} \right). \quad (\text{S.9})$$

## II. CALCULATING THE PARAMETERS OF THE ANISOTROPIC MFT

With free end-point tangent boundary conditions, the partition function

$$Z = (4\pi)^{-2} \int_S d\mathbf{u}_0 d\mathbf{u}_L \int_{\mathbf{u}(0)=\mathbf{u}_0}^{\mathbf{u}(L)=\mathbf{u}_L} D\mathbf{u} \exp(-\beta U) \quad (\text{S.10})$$

corresponding to the anisotropic MFT Hamiltonian  $U$  [Eq. (1) in the main text] can be evaluated analytically:

$$\begin{aligned} Z &= \frac{2\sqrt{2}\pi^{3/2}\beta^{-1}\epsilon_{\perp}\omega_{\perp}}{(\epsilon_{\perp}^2\omega_{\perp}^2 + 4\nu_{0\perp}^2) \sinh(L\omega_{\perp}) + 4\epsilon_{\perp}\nu_{0\perp}\omega_{\perp} \cosh(L\omega_{\perp})} \sqrt{\frac{\beta^{-1}\epsilon_{\parallel}\omega_{\parallel}}{(\epsilon_{\parallel}^2\omega_{\parallel}^2 + 4\nu_{0\parallel}^2) \sinh(L\omega_{\parallel}) + 4\epsilon_{\parallel}\nu_{0\parallel}\omega_{\parallel} \cosh(L\omega_{\parallel})}} \\ &\cdot \exp \left( \frac{\beta\chi^2 F^2 \left( \sinh\left(\frac{L\omega_{\parallel}}{2}\right) \left( \epsilon_{\parallel} L\omega_{\parallel}^2 - 4\nu_{0\parallel} \right) + 2L\nu_{0\parallel}\omega_{\parallel} \cosh\left(\frac{L\omega_{\parallel}}{2}\right) \right)}{2\epsilon_{\parallel}\omega_{\parallel}^3 \left( \epsilon_{\parallel}\omega_{\parallel} \sinh\left(\frac{L\omega_{\parallel}}{2}\right) + 2\nu_{0\parallel} \cosh\left(\frac{L\omega_{\parallel}}{2}\right) \right)} \right), \end{aligned} \quad (\text{S.11})$$

where  $\omega_{\alpha} \equiv \sqrt{2\nu_{\alpha}/\epsilon_{\alpha}}$ ,  $\alpha = \parallel, \perp$ . Similarly one can extract analytic expressions for all seven of the thermodynamic averages used in the fitting of the MFT parameters:

$$\begin{aligned} \langle R_{\parallel} \rangle &= \beta^{-1} \frac{\partial}{\partial F} \log Z, & \int_0^L ds \langle u_{\parallel}^2(s) \rangle &= -\beta^{-1} \frac{\partial}{\partial \nu_{\parallel}} \log Z, & \int_0^L ds \langle u_{\perp}^2(s) \rangle &= -\beta^{-1} \frac{\partial}{\partial \nu_{\perp}} \log Z, \\ \langle \delta R_{\parallel}^2 \rangle &= \beta^{-2} \frac{\partial^2}{\partial F^2} \log Z, & \langle \delta R_{\perp}^2 \rangle &= \frac{2}{\beta\epsilon_{\perp}\omega_{\perp}^3} \left( L\omega_{\perp} - \frac{4\nu_{0\perp}}{2\nu_{0\perp} \coth\left(\frac{L\omega_{\perp}}{2}\right) + \epsilon_{\perp}\omega_{\perp}} \right), \\ \langle u_{0\parallel}^2(0) + u_{0\parallel}^2(L) \rangle &= -\beta^{-1} \frac{\partial}{\partial \nu_{0\parallel}} \log Z, & \langle u_{0\perp}^2(0) + u_{0\perp}^2(L) \rangle &= -\beta^{-1} \frac{\partial}{\partial \nu_{0\perp}} \log Z. \end{aligned} \quad (\text{S.12})$$

By setting these expressions equal to the exact WLC results calculated from the quantum approach, Eqs. (S.8) and (S.9), one obtains a system of seven coupled equations that can be solved numerically for a given  $L$ ,  $l_p$ , and  $F$ , yielding the seven Hamiltonian parameters:  $\epsilon_{\parallel}$ ,  $\epsilon_{\perp}$ ,  $\nu_{\parallel}$ ,  $\nu_{\perp}$ ,  $\nu_{0\parallel}$ ,  $\nu_{0\perp}$ , and  $\chi$ . Fig. S.1 shows a set of solutions for  $L = 100a$ ,  $l_p = 20a$ , and varying  $F$ . In the small force regime,  $F \ll k_B T/l_p$ , where stretching is negligible, the parameters converge to the same values as in the isotropic MFT:  $\nu_{\parallel} = \nu_{\perp} = 3k_B T/4l_p$ ,  $\nu_{0\parallel} = \nu_{0\perp} = 3k_B T/4$ ,  $\epsilon_{\parallel} = \epsilon_{\perp} = 3k_B T l_p/2$  [3, 4].

## III. DYNAMICAL THEORY OF THE ANISOTROPIC MFT

Here we adapt the dynamical theory used successfully for the isotropic MFT [5, 6] to the anisotropic case of a chain under tension. The general hydrodynamic preaveraging approach is similar to that used for the Zimm model [7, 8]. The time evolution of the chain  $\mathbf{r}(s, t)$  follows the Langevin equation:

$$\frac{\partial}{\partial t} \mathbf{r}(s, t) = - \int_0^L ds' \overleftrightarrow{\boldsymbol{\mu}}(s, s'; \mathbf{r}(s, t) - \mathbf{r}(s', t)) \frac{\delta U}{\delta \mathbf{r}(s', t)} + \boldsymbol{\xi}(s, t). \quad (\text{S.13})$$

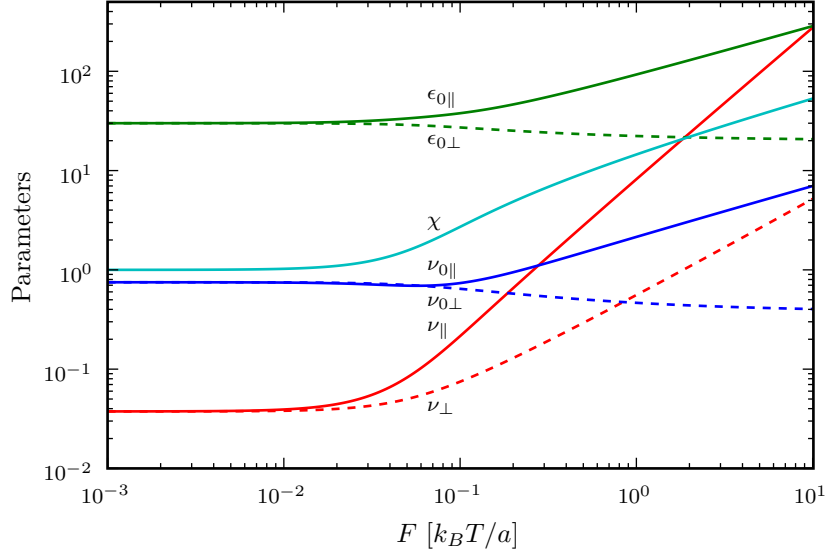


FIG. S.1: Parameters of the anisotropic MFT Hamiltonian  $U$  as a function of force  $F$  for a chain with  $L = 100a$ ,  $l_p = 20a$ , derived as described in Sec. I and II in order to reproduce exact equilibrium averages of the WLC. To plot all parameters in one graph,  $y$ -axis units have been chosen such that  $k_B T = a = 1$ .

Here the  $\xi(s, t)$  is the stochastic contribution, and  $\overleftrightarrow{\mu}(s, s'; \mathbf{x})$  is the continuum version of the Rotne-Prager tensor [5],

$$\overleftrightarrow{\mu}(s, s'; \mathbf{x}) = 2a\mu_0\delta(s - s')\overleftrightarrow{\mathbf{1}} + \Theta(x - 2a) \left( \frac{1}{8\pi\eta x} \left[ \overleftrightarrow{\mathbf{1}} + \frac{\mathbf{x} \otimes \mathbf{x}}{x^2} \right] + \frac{a^2}{4\pi\eta x^3} \left[ \frac{\overleftrightarrow{\mathbf{1}}}{3} - \frac{\mathbf{x} \otimes \mathbf{x}}{x^2} \right] \right), \quad (\text{S.14})$$

describing long-range hydrodynamic interactions between two points at  $s$  and  $s'$  on the chain contour, separated by a spatial distance  $\mathbf{x}$ . The microscopic length scale  $a$  corresponds to the monomer radius,  $\eta$  is the viscosity of water,  $\mu_0 = 1/6\pi\eta a$  is the Stokes mobility of a sphere of radius  $a$ , and the  $\Theta$  function excludes unphysical configurations (overlap between monomers).

Eq. (S.13) cannot be solved directly, because the hydrodynamic tensor depends on the exact configuration of the chain at time  $t$ , so we employ the pre-averaging approximation: replacing  $\overleftrightarrow{\mu}(s, s'; \mathbf{r}(s, t) - \mathbf{r}(s', t))$  with an average over all equilibrium configurations,  $\overleftrightarrow{\mu}_{\text{avg}}(s, s')$ :

$$\overleftrightarrow{\mu}_{\text{avg}}(s, s') = \int d^3\mathbf{x} \overleftrightarrow{\mu}(s, s'; \mathbf{x}) G(s, s'; \mathbf{x}), \quad (\text{S.15})$$

where  $G(s, s'; \mathbf{x})$  is the equilibrium probability of finding two points at  $s$  and  $s'$  with spatial separation  $\mathbf{x}$ . For the anisotropic Hamiltonian  $U$  this probability takes the form:

$$G(s, s'; \mathbf{x}) = \frac{3}{2\pi\sigma_{\perp}(s - s')} \left( \frac{3}{2\pi\sigma_{\parallel}(s - s')} \right)^{1/2} \exp \left( -\frac{3x_{\perp}^2}{2\sigma_{\perp}(s - s')} - \frac{3(x_{\parallel} - F|s - s'|/2\nu_{\parallel})^2}{2\sigma_{\parallel}(s - s')} \right), \quad (\text{S.16})$$

where  $\sigma_{\alpha}(l) \equiv (3(|l|\omega_{\alpha} + \exp(-|l|\omega_{\alpha}) - 1)/\beta\epsilon_{\alpha}\omega_{\alpha}^3)$ . In deriving  $G$  we have assumed a large chain length  $L$ , which simplifies the resulting analytical expression. Plugging Eq. (S.16) into Eq. (S.15) leads to:

$$\overleftrightarrow{\mu}_{\text{avg}}(s, s') = \begin{pmatrix} \mu_{\text{avg}}^{\perp}(s - s') & 0 & 0 \\ 0 & \mu_{\text{avg}}^{\perp}(s - s') & 0 \\ 0 & 0 & \mu_{\text{avg}}^{\parallel}(s - s') \end{pmatrix}, \quad (\text{S.17})$$

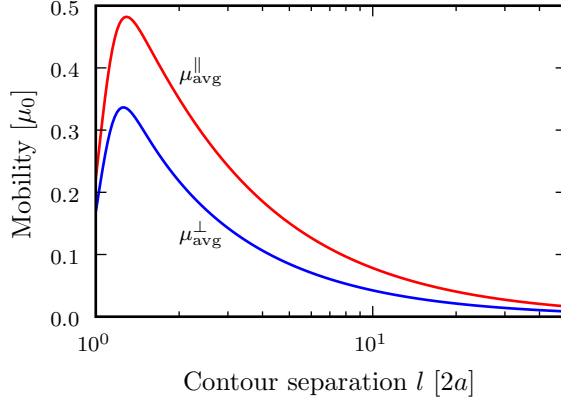


FIG. S.2: Pre-averaged mobilities  $\mu_{\text{avg}}^{\parallel}(l)$  and  $\mu_{\text{avg}}^{\perp}(l)$  as a function of contour separation  $l$  for a chain with  $L = 100a$ ,  $l_p = 20a$ , and  $F = 1.0 k_B T/a$ .

where the anisotropic mobilities  $\mu_{\text{avg}}^{\alpha}$  can be written in terms of integrals over coordinates  $x = \sqrt{x_{\perp}^2 + x_{\parallel}^2}$  and  $\zeta = x_{\parallel}/x$ :

$$\begin{aligned} \mu_{\text{avg}}^{\parallel}(l) &= 2a\mu_0\delta(l) \\ &+ \frac{3^{3/2}\Theta(l-2a)\mu_0}{(2\pi)^{3/2}\sigma_{\perp}(l)\sqrt{\sigma_{\parallel}(l)}} \int_{2a}^{\infty} dx \int_{-1}^1 d\zeta \left( \frac{\pi - 3\pi\zeta^2}{x} + \frac{3}{2}\pi(\zeta^2 + 1)x \right) \exp\left( \frac{3(\zeta^2 - 1)x^2}{2\sigma_{\perp}(l)} - \frac{3(\zeta x - Fl/2\nu_{\parallel})^2}{2\sigma_{\parallel}(l)} \right), \\ \mu_{\text{avg}}^{\perp}(l) &= 2a\mu_0\delta(l) \\ &+ \frac{3^{3/2}\Theta(l-2a)\mu_0}{(2\pi)^{3/2}\sigma_{\perp}(l)\sqrt{\sigma_{\parallel}(l)}} \int_{2a}^{\infty} dx \int_{-1}^1 d\zeta \frac{\pi(-3\zeta^2(x^2 - 2) + 9x^2 - 2)}{4x} \exp\left( \frac{3(\zeta^2 - 1)x^2}{2\sigma_{\perp}(l)} - \frac{3(\zeta x - Fl/2\nu_{\parallel})^2}{2\sigma_{\parallel}(l)} \right). \end{aligned} \quad (\text{S.18})$$

These integrals are evaluated numerically to obtain the mobilities as a function of contour distance  $l$ . In Fig. S.2 we show the results for  $L = 100a$ ,  $l_p = 20a$ , and  $F = 1.0 k_B T/a$ . Note that the mobility parallel to the stretching direction is enhanced relative to the transverse component, as we expect for an extended chain.

The pre-averaged version of the Langevin equation can now be written as:

$$\frac{\partial}{\partial t} r_{\alpha}(s, t) = - \int_0^L ds' \mu_{\text{avg}}^{\alpha}(s - s') \frac{\delta U}{\delta r_{\alpha}(s', t)} + \xi_{\alpha}(s, t), \quad (\text{S.19})$$

for  $\alpha = \parallel, \perp$ . The  $\xi(s, t)$  are Gaussian random vectors, whose components have correlations given by the fluctuation-dissipation theorem:

$$\langle \xi_{\alpha}(s, t) \xi_{\alpha}(s', t') \rangle = 2k_B T \delta(t - t') \mu_{\text{avg}}^{\alpha}(s - s'). \quad (\text{S.20})$$

Plugging in the form of  $U$ , the internal force term in the Langevin equation becomes

$$\frac{\delta U}{\delta r_{\alpha}(s', t)} = \epsilon_{\alpha} \frac{\partial^4}{\partial s'^4} r_{\alpha}(s', t) - 2\nu_{\alpha} \frac{\partial^2}{\partial s'^2} r_{\alpha}(s', t) \equiv \hat{O}_{s'}^{\alpha} r_{\alpha}(s', t), \quad (\text{S.21})$$

where we have introduced the differential operator  $\hat{O}_{s'}^{\alpha}$ . To complete the dynamical theory, we must specify the boundary conditions at the chain ends:

$$\begin{aligned} -\epsilon_{\alpha} \frac{\partial^3}{\partial s^3} r_{\alpha}(0, t) + 2\nu_{\alpha} \frac{\partial}{\partial s} r_{\alpha}(0, t) &= F\delta_{\alpha, \parallel}, & -\epsilon_{\alpha} \frac{\partial^3}{\partial s^3} r_{\alpha}(L, t) + 2\nu_{\alpha} \frac{\partial}{\partial s} r_{\alpha}(L, t) &= F\delta_{\alpha, \parallel}, \\ \epsilon_{\alpha} \frac{\partial^2}{\partial s^2} r_{\alpha}(0, t) - 2\nu_{0\alpha} \frac{\partial}{\partial s} r_{\alpha}(0, t) &= 0, & -\epsilon_{\alpha} \frac{\partial^2}{\partial s^2} r_{\alpha}(L, t) - 2\nu_{0\alpha} \frac{\partial}{\partial s} r_{\alpha}(L, t) &= 0. \end{aligned} \quad (\text{S.22})$$

The first two represent the force applied at the ends, while the second two the absence of torque. To properly deal with the boundary conditions for  $F \neq 0$ , we write  $\mathbf{r}(s, t)$  in the following way:  $r_{\alpha}(s, t) = \tilde{r}_{\alpha}(s, t) + F\delta_{\alpha, \parallel}\phi(s)$ , where



$\tilde{\mathbf{r}}(s, t)$  satisfies the homogeneous ( $F = 0$ ) version of Eq. (S.22), while  $\phi(s)$  is chosen such that the total function  $\mathbf{r}(s, t)$  satisfies the full boundary requirements. The resulting form for  $\phi(s)$  is:

$$\phi(s) = \frac{Ls}{2(L\nu_{\parallel} + 2\nu_{0\parallel})} + \frac{L\nu_{0\parallel}s^2}{2\epsilon_{\parallel}(L\nu_{\parallel} + 2\nu_{0\parallel})} - \frac{\nu_{0\parallel}s^3}{3\epsilon_{\parallel}(L\nu_{\parallel} + 2\nu_{0\parallel})}. \quad (\text{S.23})$$

We now proceed to transform the Langevin equation into matrix form, which will allow us to solve it through numerical diagonalization. Let us assume  $\xi_{\alpha}(s, t)$  satisfies similar boundary conditions to  $\tilde{r}_{\alpha}(s, t)$ , and expand both functions in normal modes  $\psi_n^{\alpha}(s)$ , with amplitudes  $p_{\alpha n}(t)$  and  $q_{\alpha n}(t)$  respectively:

$$\tilde{r}_{\alpha}(s, t) = \sum_{n=0}^{\infty} p_{\alpha n}(t) \psi_n^{\alpha}(s), \quad \xi_{\alpha}(s, t) = \sum_{n=0}^{\infty} q_{\alpha n}(t) \psi_n^{\alpha}(s). \quad (\text{S.24})$$

The normal modes  $\psi_n^{\alpha}(s)$  are chosen to be eigenfunctions of the differential operator  $\hat{O}_s^{\alpha}$ , satisfying  $\hat{O}_s^{\alpha} \psi_n^{\alpha}(s) = \lambda_{\alpha n} \psi_n^{\alpha}(s)$  for eigenvalues  $\lambda_{\alpha n}$ . These eigenfunctions take the form [5]:

$$\begin{aligned} \psi_0^{\alpha}(s) &= \sqrt{\frac{1}{L}}, \\ \psi_n^{\alpha}(s) &= \sqrt{\frac{C_{\alpha n}}{L}} \left( K_{\alpha n} \frac{\sin K_{\alpha n} s}{\cos K_{\alpha n} L/2} + G_{\alpha n} \frac{\sinh G_{\alpha n} s}{\cosh G_{\alpha n} L/2} \right), \quad n \text{ odd}, \\ \psi_n^{\alpha}(s) &= \sqrt{\frac{C_{\alpha n}}{L}} \left( -K_{\alpha n} \frac{\cos K_{\alpha n} s}{\sin K_{\alpha n} L/2} + G_{\alpha n} \frac{\cosh G_{\alpha n} s}{\sinh G_{\alpha n} L/2} \right), \quad n \text{ even}, \end{aligned} \quad (\text{S.25})$$

where

$$G_{\alpha n}^2 - K_{\alpha n}^2 = 2\nu_{\alpha}/\epsilon_{\alpha}, \quad \lambda_0^{\alpha} = 0, \quad \lambda_{\alpha n} = \epsilon_{\alpha} K_{\alpha n}^4 + 2\nu_{\alpha} G_{\alpha n}^2. \quad (\text{S.26})$$

The eigenfunctions obey the boundary conditions in the  $F = 0$  version of Eq. (S.22), which fixes the constants  $K_{\alpha n}$  and  $G_{\alpha n}$ , while the  $C_{\alpha n}$  are normalization coefficients. Plugging the normal mode expansions into the Langevin equation, and exploiting the orthonormality of the  $\psi_n^{\alpha}$ , Eqs. (S.19)-(S.20) become:

$$\begin{aligned} \frac{\partial}{\partial t} p_{\alpha n}(t) &= - \sum_{m=0}^{\infty} H_{nm}^{\alpha} \lambda_{\alpha m} p_{\alpha m}(t) + F w_n \delta_{\alpha, \parallel} + q_{\alpha n}(t), \\ \langle q_{\alpha n}(t) q_{\alpha m}(t') \rangle &= 2k_B T \delta(t - t') H_{nm}^{\alpha}, \end{aligned} \quad (\text{S.27})$$

where

$$\begin{aligned} H_{nm}^{\alpha} &= \int_0^L ds \int_0^L ds' \psi_n^{\alpha}(s) \mu_{\text{avg}}^{\alpha}(s - s') \psi_m^{\alpha}(s'), \\ w_n &= \int_0^L ds \int_0^L ds' \psi_n^{\parallel}(s) \mu_{\text{avg}}^{\parallel}(s - s') \frac{2\nu_{\parallel} \nu_{0\parallel} (L - 2s')}{\epsilon_{\parallel} (L\nu_{\parallel} + 2\nu_{0\parallel})}. \end{aligned} \quad (\text{S.28})$$

Both  $H_{nm}^{\alpha}$  and  $w_n$  can be evaluated through numerical integration. In order to make solving these equations feasible, we introduce a high-frequency cutoff  $M$  on the mode number, keeping only the slowest-relaxing modes  $n = 0, \dots, M-1$ , whose hydrodynamic interactions are described by the leading  $M \times M$  sub-blocks of the matrices  $H^{\alpha}$ . Following Ref. [6] we set  $M = L/8a$ , which provides good agreement at short times with Brownian dynamics simulations of bead-spring chains with monomer radius  $a$ . For longer times, where the polymer motion is on length scales much larger than  $a$ , the dynamical results are insensitive to the precise value of the cutoff.

The final step in simplifying the dynamical theory is diagonalization. Let  $J^{\alpha}$  be the  $M \times M$  matrix with elements  $J_{nm}^{\alpha} = H_{nm}^{\alpha} \lambda_{\alpha m}$ ,  $\Lambda_{\alpha n}$  be the eigenvalues of  $J^{\alpha}$ , and  $C^{\alpha}$  the matrix diagonalizing  $J^{\alpha}$ :  $[C^{\alpha} J^{\alpha} (C^{\alpha})^{-1}]_{nm} = \Lambda_{\alpha n} \delta_{nm}$ . Assuming non-degenerate eigenvalues  $\Lambda_{\alpha n}$ , the matrix  $C^{\alpha}$  also diagonalizes  $H^{\alpha}$  through the congruent transformation  $[C^{\alpha} H^{\alpha} (C^{\alpha})^T]_{nm} = \Theta_{\alpha n} \delta_{nm}$ , defining parameters  $\Theta_{\alpha n}$  [7]. The diagonal version of Eq. (S.27) then reads:

$$\begin{aligned} \frac{\partial}{\partial t} P_{\alpha n}(t) &= -\Lambda_{\alpha n} P_{\alpha n}(t) + F W_n \delta_{\alpha, \parallel} + Q_{\alpha n}(t), \\ \langle Q_{\alpha n}(t) Q_{\alpha m}(t') \rangle &= 2k_B T \delta(t - t') \delta_{m, n} \Theta_{\alpha n}, \end{aligned} \quad (\text{S.29})$$

where

$$P_{\alpha n}(t) = \sum_{m=0}^{M-1} C_{nm}^{\alpha} p_{\alpha m}(t), \quad Q_{\alpha n}(t) = \sum_{m=0}^{M-1} C_{nm}^{\alpha} q_{\alpha m}(t), \quad W_n = \sum_{m=0}^{M-1} C_{nm}^{\parallel} w_m, \quad (\text{S.30})$$

and  $r_{\alpha}(s, t) = \sum_n P_{\alpha n}(t) \Psi_n^{\alpha}(s) + F \delta_{\alpha, \parallel} \phi(s)$  with modified normal modes  $\Psi_n^{\alpha}(s) = \sum_m \psi_m^{\alpha}(s) [(C^{\alpha})^{-1}]_{mn}$ . Using Eq. (S.29) it now becomes possible to solve for a variety of dynamical observables. For example, the result for the MSD of a chain end-point is:

$$\begin{aligned} \Delta_{\alpha}^{\text{end}}(t) &\equiv \langle (r_{\alpha}(L, t) - r_{\alpha}(L, 0))^2 \rangle = 2k_B T \left[ \Theta_{\alpha 0} (\Psi_0^{\alpha}(L))^2 t + \sum_{n>0} \frac{\Theta_{\alpha n}}{\Lambda_{\alpha n}} (1 - \exp(-\Lambda_{\alpha n} t)) (\Psi_n^{\alpha}(L))^2 \right] \\ &= 2D_{\alpha} t + 2k_B T \sum_{n>0} A_{\alpha n}^{\text{end}} (1 - \exp(-\Lambda_{\alpha n} t)), \end{aligned} \quad (\text{S.31})$$

where we have introduced the center-of-mass diffusion constant  $D_{\alpha} = k_B T \Theta_{\alpha 0} (\Psi_0^{\alpha}(L))^2$ , and coefficients  $A_{\alpha n}^{\text{end}} = \Theta_{\alpha n} (\Psi_n^{\alpha}(L))^2 / \Lambda_{\alpha n}$ . Similarly, for the MSD of the end-to-end vector,

$$\begin{aligned} \Delta_{\alpha}^{\text{ee}}(t) &\equiv \langle (R_{\alpha}(t) - R_{\alpha}(0))^2 \rangle = 2k_B T \sum_{n>0} \frac{\Theta_{\alpha n}}{\Lambda_{\alpha n}} (1 - \exp(-\Lambda_{\alpha n} t)) (\Psi_n^{\alpha}(L) - \Psi_n^{\alpha}(0))^2 \\ &= 2k_B T \sum_{n>0} A_{\alpha n}^{\text{ee}} (1 - \exp(-\Lambda_{\alpha n} t)), \end{aligned} \quad (\text{S.32})$$

where  $A_{\alpha n}^{\text{ee}} = \Theta_{\alpha n} (\Psi_n^{\alpha}(L) - \Psi_n^{\alpha}(0))^2 / \Lambda_{\alpha n}$ .

#### IV. BROWNIAN DYNAMICS SIMULATIONS

For the BD simulations [9] used to validate the mean-field theory, the chain consists of  $N$  beads of radius  $a$  whose positions  $\mathbf{r}_i(t)$  are governed by the discrete Langevin equation:

$$\frac{d\mathbf{r}_i(t)}{dt} = \sum_{j=1}^N \overleftrightarrow{\boldsymbol{\mu}}_{ij} \cdot \left( -\frac{\partial U(\mathbf{r}_1, \dots, \mathbf{r}_N)}{\partial \mathbf{r}_j} \right) + \boldsymbol{\xi}_i(t). \quad (\text{S.33})$$

Long-range hydrodynamic interactions between monomers are included through the Rotne-Prager [10] mobility matrix  $\overleftrightarrow{\boldsymbol{\mu}}_{ij}$ :

$$\overleftrightarrow{\boldsymbol{\mu}}_{ij} = \mu_0 \delta_{i,j} \overleftrightarrow{\mathbf{1}} + (1 - \delta_{i,j}) \left( \frac{1}{8\pi\eta r_{ij}} \left[ \overleftrightarrow{\mathbf{1}} + \frac{\mathbf{r}_{ij} \otimes \mathbf{r}_{ij}}{r_{ij}^2} \right] + \frac{a^2}{4\pi\eta r_{ij}^3} \left[ \frac{\overleftrightarrow{\mathbf{1}}}{3} - \frac{\mathbf{r}_{ij} \otimes \mathbf{r}_{ij}}{r_{ij}^2} \right] \right), \quad (\text{S.34})$$

where  $\mathbf{r}_{ij} \equiv \mathbf{r}_i - \mathbf{r}_j$ . This matrix also determines correlations for the Gaussian stochastic velocities  $\boldsymbol{\xi}_i(t)$  according to the fluctuation-dissipation theorem:

$$\langle \boldsymbol{\xi}_i(t) \otimes \boldsymbol{\xi}_j(t') \rangle = 2k_B T \overleftrightarrow{\boldsymbol{\mu}}_{ij} \delta(t - t'). \quad (\text{S.35})$$

The elastic potential of the chain  $U = U_{\text{ben}} + U_{\text{str}} + U_{\text{LJ}} + U_{\text{ext}}$  consists of four parts: (i) a bending energy  $U_{\text{ben}} = (\epsilon/2a) \sum_i (1 - \cos \theta_i)$ , where  $\theta_i$  is the angle between two adjacent bonds, and  $\epsilon$  is related to the persistence length  $l_p$  as  $\epsilon = l_p k_B T$ ; (ii) a harmonic stretching term  $U_{\text{str}} = (\gamma/4a) \sum_i (r_{i+1,i} - 2a)^2$  where inextensibility is enforced through a large modulus  $\gamma = 2000 k_B T/a$ ; (iii) a truncated Lennard-Jones interaction  $U_{\text{LJ}} = \omega \sum_{i<j} \Theta(2a - r_{ij}) [(2a/r_{ij})^{12} - 2(2a/r_{ij})^6 + 1]$  with  $\omega = 3k_B T$ ; (iv) an external force  $F$  along the  $z$  direction,  $U_{\text{ext}} = -F \hat{\mathbf{z}} \cdot (\mathbf{r}_N - \mathbf{r}_1)$ .

In the numerical implementation of Eq. (S.33), the Langevin time step is  $\tau = 3 \times 10^{-4} a^2 / (k_B T \mu_0)$ , where  $\mu_0$  is the Stokes mobility of a monomer, and a typical simulation lasts  $\sim 10^8 - 10^9$  steps. Data is collected every  $10^2 - 10^3$  steps, and averages for the dynamical quantities discussed in the main text are based on 5-25 independent runs.

## V. RESULTS FOR REAL AND IMAGINARY PARTS OF RESPONSE FUNCTIONS

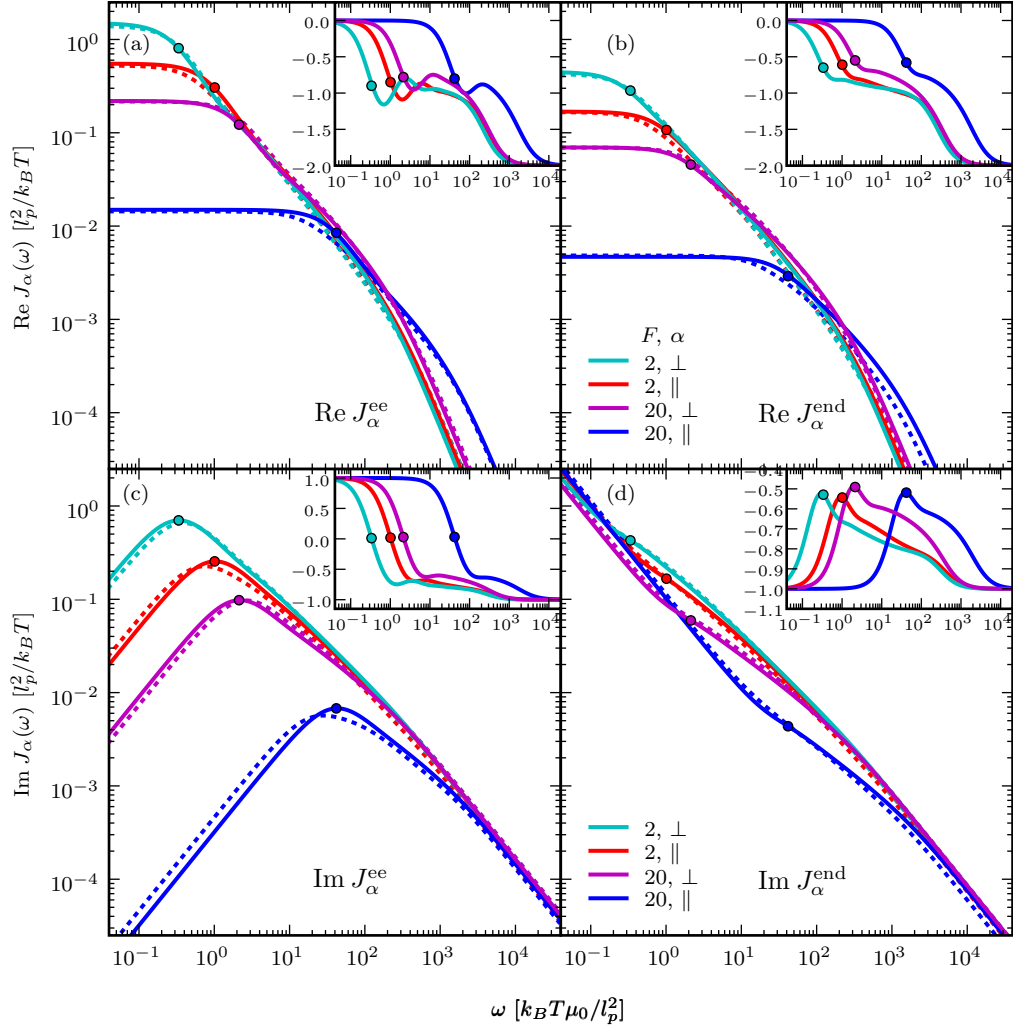


FIG. S.3: For a polymer with  $L = 100a$ ,  $L/l_p = 5$ : (a)  $\text{Re } J_\alpha^{\text{ee}}(\omega)$ ; (b)  $\text{Re } J_\alpha^{\text{end}}(\omega)$ ; (c)  $\text{Im } J_\alpha^{\text{ee}}(\omega)$ ; (d)  $\text{Im } J_\alpha^{\text{end}}(\omega)$ . Solid lines are the anisotropic MFT results, while dashed lines are taken from BD simulations. In all cases results are given for  $\alpha = \perp, \parallel$  at two forces,  $F = 2$  and  $20 k_B T/l_p$ . Filled circles mark the relaxation times  $\tau_{\alpha 1}$ , derived from the MFT, while the insets show the local slopes of the MFT curves in the log-log plots.

## VI. WEAKLY BENDING APPROXIMATION FOR $\Delta_\parallel^{\text{ee}}(t)$ BASED ON THE $\perp$ MFT RESULTS

For small deviations from the rigid rod limit, the  $\parallel$  and  $\perp$  tangent vectors of the WLC can be related as:  $u_\parallel(s, t) = \sqrt{1 - \mathbf{u}_\perp^2(s, t)} \approx 1 - \mathbf{u}_\perp^2(s, t)/2 - \mathbf{u}_\perp^4(s, t)/8 + \dots$ , where  $\mathbf{u}_\perp = (u_x, u_y)$ . This is the fundamental equation for the weakly bending approximation, and it allows one to derive certain aspects of the  $\parallel$  dynamics assuming the  $\perp$  dynamics are known, specifically the behavior of  $\mathbf{u}_\perp^2(s, t)$ . As seen in Fig. 3(b) of the main text, the anisotropic MFT provides a highly accurate prediction for the  $\perp$  end-to-end MSD even for very stiff chains, so we can exploit the reliability of the  $\perp$  dynamical theory through the WBA approach.

We focus on finding an estimate for the  $\parallel$  end-to-end MSD function  $\Delta_\parallel^{\text{ee}}(t)$ , though the method is generalizable to other dynamical quantities.  $\Delta_\parallel^{\text{ee}}(t)$  can be expressed as  $\Delta_\parallel^{\text{ee}}(t) = 2(C_\parallel(0) - C_\parallel(t))$ , where the correlation function

$C_{\parallel}(t)$  is given by:

$$C_{\parallel}(t) = \langle R_{\parallel}(t)R_{\parallel}(0) \rangle - \langle R_{\parallel} \rangle^2 = \int_0^L ds \int_0^L ds' \langle u_{\parallel}(s,t)u_{\parallel}(s',0) \rangle - \left[ \int_0^L ds \langle u_{\parallel}(s,0) \rangle \right]^2. \quad (\text{S.36})$$

Here we have used the fact that  $R_{\parallel}(t) = \int_0^L ds u_{\parallel}(s,t)$ . Plugging in the second-order expansion  $u_{\parallel}(s,t) \approx 1 - \mathbf{u}_{\perp}^2(s,t)/2 - \mathbf{u}_{\perp}^4(s,t)/8$ , we get an expression for  $C_{\parallel}(t)$  involving averages over various products of  $\mathbf{u}_{\perp}^2(s,t)$ . From the normal mode expansion in Sec. III we know that  $\mathbf{u}_{\perp}(s,t) = \partial_s \mathbf{r}_{\perp}(s,t) = \sum_n \mathbf{P}_{\perp n}(t) \Psi_n^{\perp'}(s)$ , where  $\mathbf{P}_{\perp n} = (P_{xn}, P_{yn})$  and  $\Psi_n^{\perp'}(s) \equiv \partial_s \Psi_n^{\perp}(s)$ . Thus all averages over  $\mathbf{u}_{\perp}^2(s,t)$  are averages over the normal mode amplitudes  $\mathbf{P}_{\perp n}(t)$ , and these can be directly calculated from Wick's theorem and the solution of Eq. (S.29) for the  $\perp$  components. The final result for  $C_{\parallel}(t)$  at order  $\mathcal{O}(\mathbf{u}_{\perp}^4)$  has the form:

$$C_{\parallel}(t) = \sum_{k,l} f_k(t) f_l(t) M_{kl}^2 + 4 \sum_{k,l,m} f_k(t) f_l(t) f_m(0) M_{kl} M_{mmkl} + \sum_{k,l,m,n} f_k(t) f_l(t) f_m(t) f_n(t) M_{klmn}^2 + 4 \sum_{k,l,m,n} f_k(t) f_l(t) f_m(0) f_n(0) M_{klmm} M_{klmn}, \quad (\text{S.37})$$

where:

$$\begin{aligned} f_k(t) &= \frac{k_B T \Theta_{\perp k}}{\Lambda_{\perp k}} \exp(-\Lambda_{\perp k} t), \\ M_{kl} &= \int_0^L ds \Psi_k^{\perp'}(s) \Psi_l^{\perp'}(s), \\ M_{klmn} &= \int_0^L ds \Psi_k^{\perp'}(s) \Psi_l^{\perp'}(s) \Psi_m^{\perp'}(s) \Psi_n^{\perp'}(s). \end{aligned} \quad (\text{S.38})$$

Thus  $C_{\parallel}(t)$  can be expressed entirely in terms of quantities from the  $\perp$  MFT solution: the parameters  $\{\Lambda_{\perp n}, \Theta_{\perp n}\}$  and the normal modes  $\{\Psi_n^{\perp}(s)\}$ . Numerical evaluation of Eqs. (S.37)-(S.38) yields  $C_{\parallel}(t)$  and hence  $\Delta_{\parallel}^{\text{ee}}(t)$ .

- 
- [1] N. Saito, W. Takahashi, and Y. Yunoki, J. Phys. Soc. Japan **22**, 219 (1967).
  - [2] J. Samuel and S. Sinha, Phys. Rev. E **66**, 050801 (2002).
  - [3] R. G. Winkler, P. Reineker, and L. Harnau, J. Chem. Phys. **101**, 8119 (1994).
  - [4] B. Y. Ha and D. Thirumalai, J. Chem. Phys. **103**, 9408 (1995).
  - [5] L. Harnau, R. G. Winkler, and P. Reineker, J. Chem. Phys. **104**, 6355 (1996).
  - [6] M. Hinczewski et al., Macromol. **42**, 860 (2009).
  - [7] B. H. Zimm, J. Chem. Phys. **24**, 269 (1956).
  - [8] M. Doi and S. F. Edwards, *The Theory of Polymer Dynamics* (Oxford University Press, USA, 1988).
  - [9] D. L. Ermak and J. A. McCammon, J. Chem. Phys. **69**, 1352 (1978).
  - [10] J. Rotne and S. Prager, J. Chem. Phys. **50**, 4831 (1969).
-